Optical diagnostics for high electron density plasmas

OPTICAL DIAGNOSTICS FOR HIGH ELECTRON DENSITY PLASMAS

M.C.M. van de Sanden, R.F.G. Meulenbroeks, J.J. Beulens,
A.J.M. Buuron, M.J. de Graaf, G.J. Meeusen, Z. Qing,
J.M. de Regt, Gh. Dinescu, D.K. Otorbaev and D.C. Schram

Department of Physics, Eindhoven University of Technology
P.O.Box 513, 5600 MB Eindhoven, The Netherlands

INTRODUCTION

Nowadays high electron density plasmas are, beside their fundamental interest, widely used for many applications, e.g., light sources and plasma processing. The well known examples of high electron density plasmas can be found among the class of thermal plasmas as, e.g., the Inductively Coupled Plasma (ICP) and the Wall Stabilized Cascaded Arc (WSCA). Usually the pressure of the plasma is high, i.e., sub atmospheric to atmospheric. Other examples are the plasmas generated in tokamaks for fusion purposes and the recently exploited plasmas for etching and deposition devices such as the Electron Cyclotron Resonance plasmas. For the plasmas mentioned, the electron density is typical in the range of 10^{18} to 10^{23} m^{-3}, and the electron velocity distribution is close to a Maxwellian velocity distribution.

The relatively high electron density makes the application of certain specific diagnostics possible. Since these type of plasmas emit light, passive techniques as Optical Emission Spectroscopy and Fabry-Pérot Interferometry become a relatively easy way to gain information about the plasma. Active diagnostics like Thomson scattering, which are difficult if the electron density is below 10^{18} m^{-3}, give a powerful means of determining essential plasma parameters as the electron density and temperature locally in the plasma.

The outline of the paper is as follows. Three optical diagnostics will be discussed. These three diagnostics are a combined Thomson-Rayleigh scattering, Optical Emission Spectroscopy and Fabry-Pérot Interferometry. The results presented throughout this paper are obtained at one type of argon plasma (see fig. 1), i.e. the plasma expanding from a wall stabilized cascaded arc into a low background pressure. When this plasma is used for high rate deposition of amorphous hydrogenated carbon or silicon layers [1,2], monomers as CH_4 or SiH_4 are injected. In the case that the plasma is used as a hydrogen atom or ion source (H^+ or H^-) [3], H_2 is injected in the argon plasma jet or the cascaded arc is operated on H_2.

Microwave Discharges: Fundamentals and Applications
Edited by C.M. Ferreira and M. Moisan, Plenum Press, New York, 1993

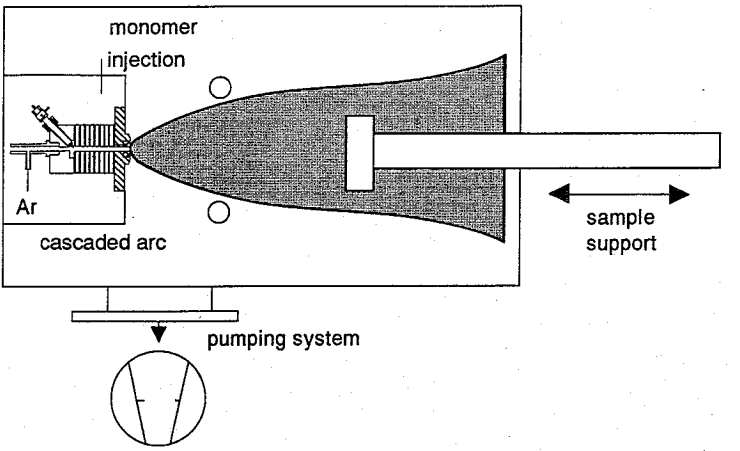

Figure 1. The plasma expanding from a cascaded arc.

COMBINED THOMSON-RAYLEIGH SCATTERING

A method to determine the electron density and temperature in a plasma is Thomson scattering [4,5]. Thomson scattering is the scattering of light by free electrons [4]. The advantage is that the electron density and temperature are measured locally and that no model assumptions are necessary. Unfortunately Thomson scattering is very weak and only when powerful lasers became available, Thomson scattering became popular [5]. A method related to Thomson scattering is Rayleigh scattering which is the scattering of bound electrons of atoms and ions. It is used to determine the neutral particle density locally [6]. A key problem here is the stray light because one can not distinguish it from the Rayleigh scattering signal. Combining the two scattering diagnostics in one set up is very convenient in studying plasmas, because the three important plasma parameters can be measured simultaneously. Recently set ups which combine the two scattering techniques were developed [7,8].

Since there is an extensive literature both on Thomson and Rayleigh scattering [4,5,9] only the main features are presented here. In fig. 2 the scattering geometry of the Thomson-Rayleigh

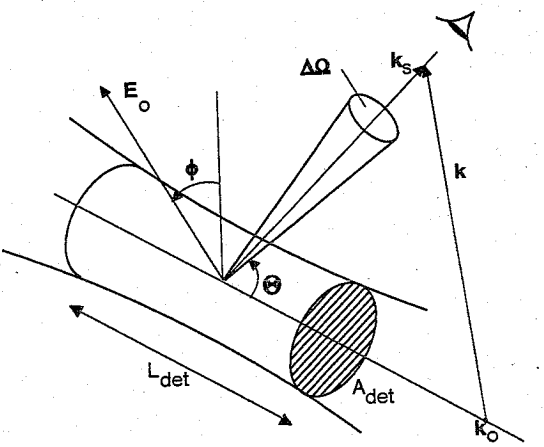

Figure 2. The scattering geometry.

experiment is depicted. The Doppler shift of the frequency of the scattered radiation is a result of two effects:

- The incident wave is "seen" by the charged particle at a Doppler-shifted frequency, because the particle is moving with respect to the source of radiation.
- The particle has a velocity component in the direction of the observer which gives a second Doppler shift.

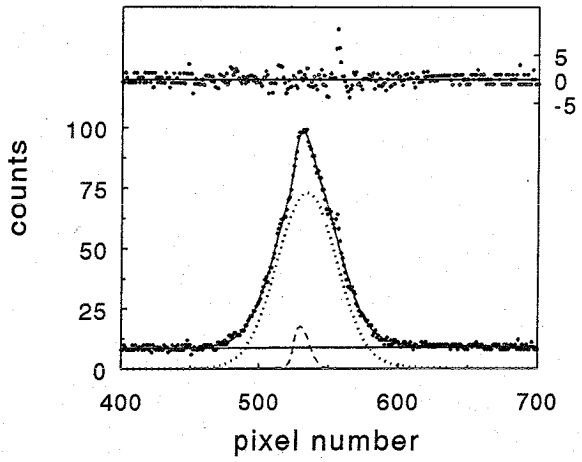

Figure 3. A measured Thomson-Rayleigh profile with least mean square fit and 5 × magnified residue.

The frequency shift $\Delta\omega$ is defined as

$$\Delta\omega = \omega_s - \omega_0 = (\mathbf{k}_s - \mathbf{k}_0) \cdot \mathbf{v} = \mathbf{k} \cdot \mathbf{v}, \tag{1}$$

i.e., the frequency shift $\Delta\omega$ is proportional to the component of the particle velocity in the direction of the scattering vector $\mathbf{k}$. If the scattering electrons in the detection volume are free electrons the scattering phenomenon is called Thomson scattering. Here the scattering parameter is introduced as $\alpha = (k\lambda_d)^{-1}$ with λ_d the Debye length, and k the length of the scattering vector. Now two cases can be considered:

- If $\lambda_0/(4\pi \sin(\theta/2)) \ll \lambda_d$, which means $\alpha \ll 1$. This is incoherent Thomson scattering. The incident wave "sees" the individual electrons, which appear free. In this case the scattered spectrum reflects the shape of the electron velocity distribution (this follows from Eq. (1))
- If $\lambda_0/(4\pi \sin(\theta/2)) \geq \lambda_d$, which means $\alpha \geq 1$, we have coherent scattering. The incident wave now interacts with shielded charges. The scattered spectrum therefore depends on the collective behavior of groups of charges.

The Thomson scattering set up described further on in this paper has a scattering parameter which is in the range $\alpha < 1$ but not $\alpha \ll 1$. This case is more complicated than the case of incoherent scattering [7], which, however, we will not discuss here.

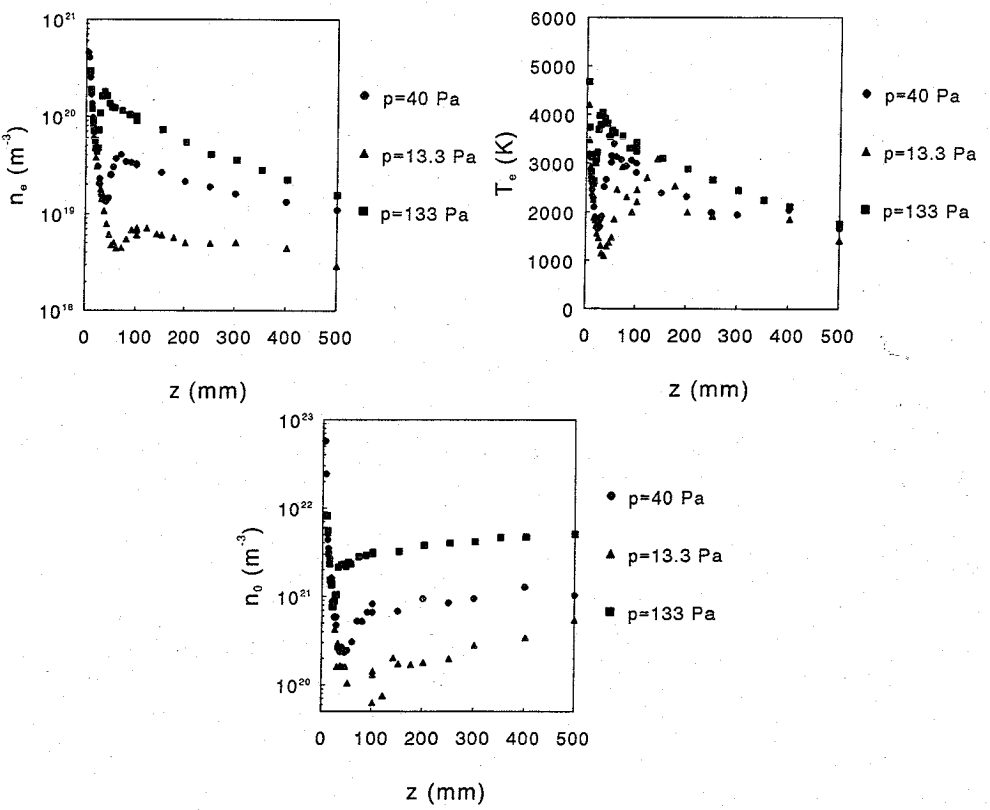

Figure 4: n_e (top left), T_e (top right) and n_0 (bottom) on the axis as a function of the axial position for different background pressures. $I_{cas} = 45$ A, $Ar - flow = 3500$ ml/min.

The general expression for the scattered power in a solid angle $d\Omega_s$ and in a frequency range $d\omega_s$ $(= d\omega)$ for Thomson scattering is given by [4,5,9]

$$P_s^T d\omega_s = P_0 n_e L S(\mathbf{k},\omega) \frac{d\sigma_T}{d\Omega} d\Omega_s d\omega_s, \tag{2}$$

where P_s^T and P_0 are the scattered and incident power respectively, $\frac{d\sigma_T}{d\Omega}$ is the differential cross section for Thomson scattering $(= r_e^2$ with $r_e = \frac{e}{4\pi\epsilon_0 m_e c^2} = 2.82 \cdot 10^{-15}$ m, the classical electron radius) and L is the length of the scattering volume. That Thomson scattering is weak is expressed by the smallness of the cross section $(= 7.95 \cdot 10^{-30}$ m$^2)$. In Eq. (2) the scattering geometry is chosen for which the scattered signal is maximum, i.e., $\phi = \theta = 90^o$ (see fig. 2). For a typical scattering experiment $P_s^T/P_0 \approx 10^{-14}$. In Eq. (2) $S(\mathbf{k},\omega)$ is the spectral density function reflecting the influence of the electron velocity distribution. In the case of a Maxwellian velocity distribution and $\alpha \ll 1$, $S(\mathbf{k},\omega)$ is given by

$$S(\mathbf{k},\omega) = \frac{F_e(\frac{\omega}{k})}{k} = \frac{1}{(\pi k v_e)^{\frac{1}{2}}} \exp(-(\frac{\omega}{k v_e})^2), \tag{3}$$

with $F_e(\frac{\omega}{k})$ the one-dimensional Maxwellian distribution function of the electrons parallel to $\mathbf{k}$ and $v_e = \sqrt{\frac{2k_b T_e}{m_e}}$ the thermal speed of the electrons in the scattering plane. Note that $S(\mathbf{k},\omega)$ is normalized. The more complicated case of the calculation of $S(\mathbf{k},\omega)$ to order α^2, using the Salpeter approximation [10] is treated elsewhere [7]. In the case of incoherent scattering, the scattered spectrum is purely Gaussian (cf. Eq. (3)). It is easily seen that n_e is proportional to the area under the Gaussian profile. The electron temperature T_e is calculated from the $\frac{1}{e}$ width $\Delta\lambda_{\frac{1}{e}}$ of the Gaussian profile. In the incoherent case the scattered spectra is directly proportional to the velocity distribution in the scattering plane.

The expression for the scattered power for Rayleigh scattering is similar to that for Thomson scattering [7,8] (cf. Eq. (2)). The scattered power is given by

$$P_s^R d\omega_s = P_0(n_0 + \beta n_i) L \delta(\omega) \frac{d\sigma_R}{d\Omega} d\Omega_s d\omega_s, \tag{4}$$

with $\frac{d\sigma_R}{d\Omega}$ the differential cross section for Rayleigh scattering. The ratio between the differential Rayleigh cross sections of the ions and neutral particles is given by β, which for argon [8] is equal to $\beta = 0.393$. The ratio of the differential Rayleigh and Thomson cross sections for argon, for an incident wavelength of 532 nm is given by χ (the Rayleigh cross section has, in contrast to the Thomson cross section, a λ^{-4} wavelength dependency [9]). χ is given by Jauernik et al. [8] and equals $\chi = 1/143$ for argon. The Doppler width of the scattered spectrum is proportional to $m^{-1/2}$, where in this case m is the mass of the atoms. This means that the width of the Rayleigh profile is small compared to the Thomson profile, so that the spectral density function in the Rayleigh case can be approximated by a Dirac δ-function.

To summarize: in a combined Thomson-Rayleigh scattering experiment the broad Thomson spectrum can be easily distinguished from the small Rayleigh peak which is superimposed on top of the Thomson profile. The Thomson profile can be used to determine the electron density and temperature while the Rayleigh peak is proportional to the neutral particle density.

In this paper the discussion will be focused on a combined Thomson and Rayleigh scattering set up developed at the Eindhoven University [7]. As already mentioned a key problem in designing a combined Thomson-Rayleigh scattering set up is the level of the stray light. The level in this set up is diminished to 0.4 Pa argon at 300 K stray light equivalent, making it possible to measure neutral particle densities down to 10^{20} m^{-3}. The main components of the set up are a frequency doubled Nd:YAG laser ($\lambda_0 = 532$ nm), a polychromator to disperse the

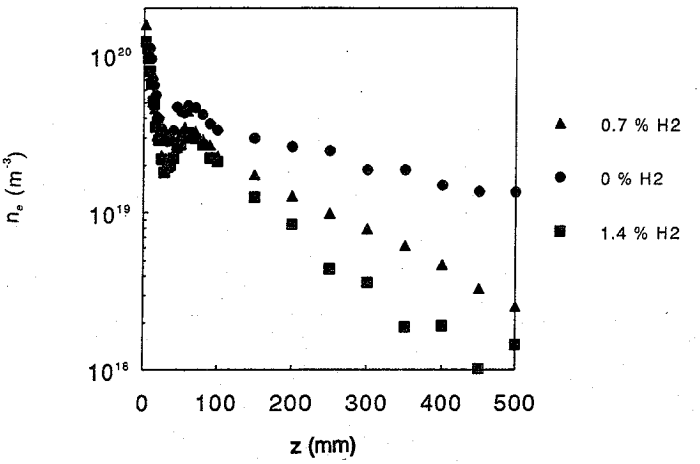

Figure 5. n_e on the axis as a function of the axial position for different percentage of hydrogen flow. $I_{cas} = 45$ A, $Ar - flow = 3500$ ml/min, $p = 40$ Pa.

scattered signal and a detector. Important is that the detector consists of a gated light amplifier in combination with a photo diode array. This combination has a nearly single photon counting ability.

To deduce absolute results from the Thomson-Rayleigh spectra, the set up needs to be calibrated relatively and absolutely. The relative calibration of the detector channels (pixels) is done using a tungsten ribbon lamp. The absolute calibration is performed on an argon gas sample (typically 200 Pa). From the ratio between the Rayleigh and the Thomson cross section, the measured pressure and temperature of the gas sample, a relation can be determined between the density and the amount of signal. The absolute calibration is also used for another purpose, i.e. the determination of the instrumental profile of the detector. This instrumental profile is then in turn used to analyze the measured spectra by convolution techniques as is discussed by van de Sanden et al. [7]. In this way the accuracy and dynamic range of the set up are significantly increased. Typical values of the accuracies in n_e are 1 to 4%, for T_e 2 to 6% and for n_0 10 to 50% respectively, depending on the plasma conditions.

In fig. 3 a typical measured Thomson-Rayleigh profile is given. Also the least mean square fit is shown and the five times magnified residue. The small Rayleigh peak on top of the broadened Thomson profile can be clearly seen. In fig. 4 the axial profiles of n_e, T_e and n_0 are given as a function of the axial position in the plasma jet for different background pressures. The supersonic expansion and the stationary shock front can be clearly seen. Figure 5 gives n_e as a function of the axial position for different hydrogen flow percentages added to the main argon flow. Clearly the influence of H_2 on n_e can be seen. If no hydrogen is present n_e remains relatively high whereas it decreases rapidly if hydrogen is present [11]. The explanation for this observation is the recirculation of H_2 in the vacuum vessel which by charge exchange and subsequently dissociative recombination of the formed ArH^+ molecule destructs the electron density [3,11,12]. Later on we will see the same phenomena for other monomers.

OPTICAL EMISSION SPECTROSCOPY

The excited state densities of atomic species can be determined from line intensity measurements. This passive spectroscopic technique is important in equilibrium studies [13,14]. It

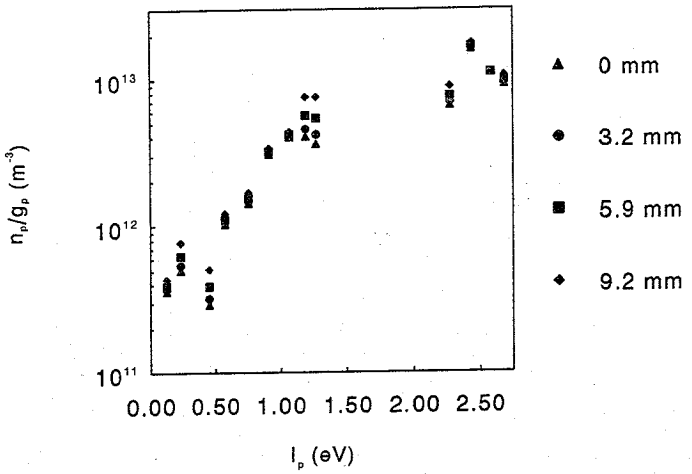

Figure 6. $\frac{n_p}{g_p}$ as a function of the ionization potential I_p for different radial positions at $z = 40$ mm. $I_{cas} = 45$ A, $Ar - flow = 3500$ ml/min, $p = 40$ Pa.

becomes even more powerful, if it is combined with an independent method to determine the electron density and electron temperature (e.g. Thomson scattering). Then it is possible from the distribution of these excited state densities with respect to the ionization energy of the state to determine whether the plasma is in a certain specific equilibrium. Furthermore, the excited state densities can be used to estimate the recombination or ionization rate [14]. If the electron density and temperature are not available, absolute line intensity measurements are still very useful and give insight in the kinetics of the plasma [2].

The radiated power P_{pq}, emitted by n_p excited particles per unit volume per unit solid angle in some upper state p, which decay to some lower state q by spontaneous emission, in the absence of stimulated or absorption effects, is given by

$$P_{pq} = (4\pi)^{-1} n_p A_{pq} h\nu_{pq}, \tag{5}$$

where A_{pq} is the transition probability and $h\nu_{pq}$ is the photon energy. Measurement of the absolute value of P_{pq} gives, provided that A_{pq} is known, the absolute value of the excited state density n_p.

Since OES is non local, an Abel inversion (in case of cylinder symmetry) is performed to get local information from a lateral profile. Several techniques were used in the past, as, e.g., direct integration of the Abel integral, expansion techniques or the more recently employed technique of tomographic Abel inversion. This last technique has the advantage that it is a fast and reliable method with at least the same accuracy as the other two mentioned.

In fig. 6 a typical example is given of the measured $\frac{n_p}{g_p}$ as a function of the ionization potential I_p of the level p for the recombining plasma jet in argon [16]. The slope of the highest levels could reveal the electron temperature, however, the accuracy of the determined excited state density is rather poor, so that the obtained a temperature has a large uncertainty. The electron density, however, can be obtained with a reasonable accuracy from an extrapolation to the continuum using the Saha equation. The Saha equation is given by

$$(\frac{n_p^S}{g_p^S})^{Saha} = \frac{n_e n_+^S}{2g_+^S} \frac{h^3}{(2\pi m_e k_b T_e)^{\frac{3}{2}}} \exp(\frac{I_p^S}{k_b T_e}), \tag{6}$$

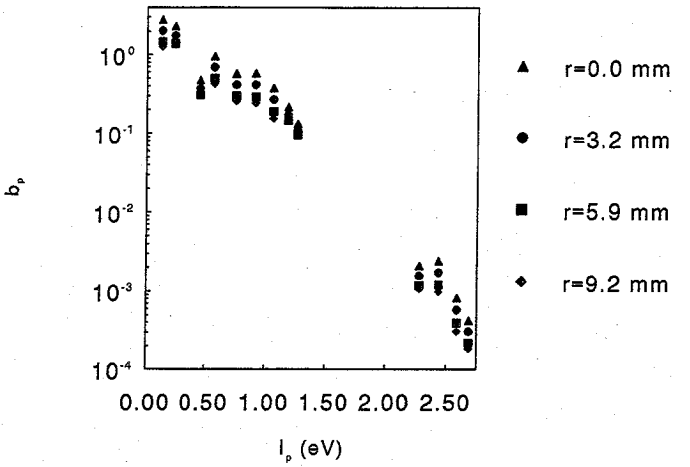

Figure 7. b_p as a function of the ionization potential I_p (see fig. 6).

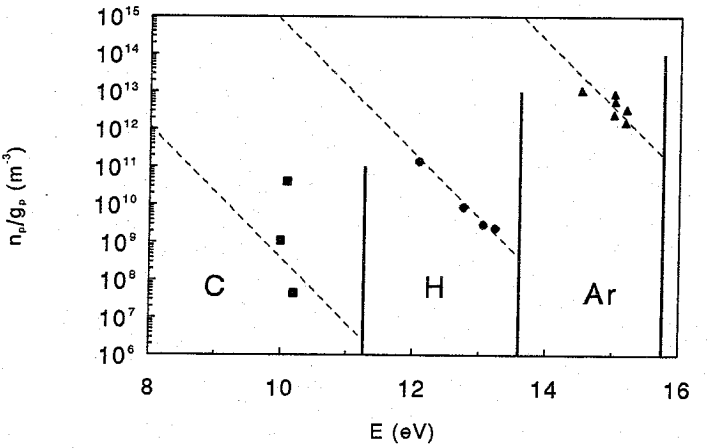

Figure 8. $\frac{n_p}{g_p}$ as a function of the ionization potential I_p for the different species C, H and Ar.

where the superscript S is used to denote the specie S, n_+^S is the ion ground state of the specie S, and I_p^S is the ionization potential of the level p of the specie S. Using Eq. (6) for argon and the Thomson scattering results, the overpopulation factor b_p [13,14] can be calculated. The b_p-factor reflects the departure of Saha equilibrium of the specific state. The b_p-factor is defined as

$$b_p = \frac{n_p}{n_p^{Saha}}. \qquad (7)$$

In fig. 7 the corresponding b_p-factors are given for the same condition as fig. 6. Immediately it can be seen that the highly excited states are in equilibrium with the continuum ($b_p \approx 1$) and that the lower excited states are strongly under populated. From this it can be concluded that the plasma in this case is recombining and from the gradient in b_p the recombination flow can in principle be determined [14,16]. Figure 8 shows similar measurements of $\frac{n_p}{g_p}$ for the different species in an argon plasma with CH_4 admixed. If the presence of other ionic species can be neglected and using the assumption that the electron temperature is equal to the determined

vibrational temperature, which is determined from the CH radical emission, the different ion densities of n_+^C, n_+^H, n_+^{Ar} and n_e can be determined using quasi-neutrality [17]. In fig. 9 the result for the determined n_e for different CH_4 flows admixed to the main argon flow is shown. Again the reason for the destruction of the ionization degree for an increasing amount of monomer flow of CH_4 is the chain of charge exchange between Ar^+ ions and the CH_x (with x=2...4) molecules forming molecular ions and the dissociative recombination of this molecular ion with an electron [17]. Effectively the ionization degree is lost by this mechanism.

The demonstrated OES for a recombining high electron density plasma reveals one large difference with for example RF generated plasmas. The latter type of plasma, due to the relatively high electron temperature ($T_e = 2 - 4$ eV) is usually ionizing. As a consequence

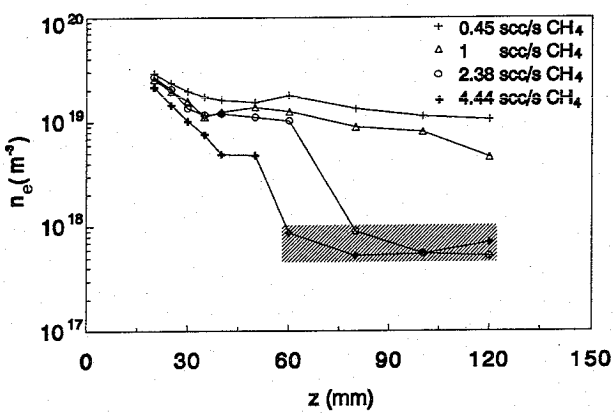

Figure 9. n_e as a function of axial position for different CH_4 flows admixed in the main argon flow.

a corona model for the lower excited states is applicable [14]. The light emission is due to the electronic excitation from the ground state. Information employing OES in this case gives information over the lower excited states. Contrary to this is the high electron density recombining plasma, which shows another feature. The highly excited states are in Saha equilibrium and here the light emission is mainly due to the recombination to the highly excited states. Performing OES in this case reveals information on the ion ground state and the electron gas.

FABRY-PÉROT INTERFEROMETRY

The heavy particle temperatures in plasmas can be measured using Fabry-Pérot Interferometry [18]. The principle of these measurements is the broadening of spectral lines. Usually two broadening mechanisms are important for high electron density plasmas. These two mechanisms are Doppler broadening due the thermal motion of the particles and Stark broadening which is caused by the presence of charges in plasmas. Besides this the spectral line can also be shifted because of drift and rotational velocities and due to the Stark effect (Stark shift).

If the velocity distribution of the heavy particles is Maxwellian, the Doppler broadening results in a Gaussian profile and the temperature can be calculated from the $\frac{1}{e}$ width. The Stark broadening on the other hand results in a Lorentzian profile. For almost all spectral lines (except hydrogen), the Stark broadening and shift are linear in the electron density [18]. If the

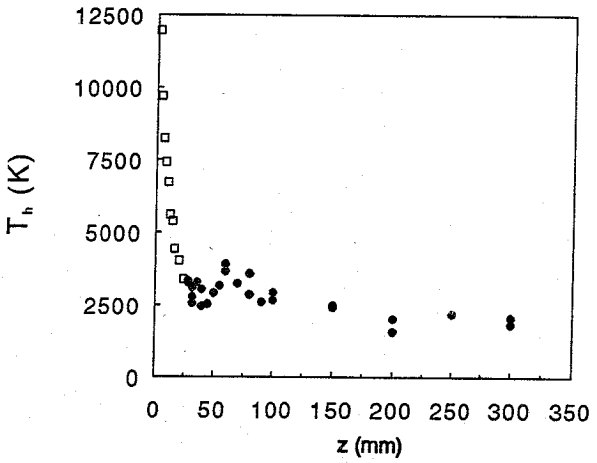

Figure 10. T_h as a function of the axial position. $I_{cas} = 45$ A, $Ar - flow = 3500$ ml/min, $p = 40$ Pa. □ : 415.9 nm and • : 696.5 nm.

two broadening mechanism occur simultanously, the resulting line profile is a Voigt profile. Griem [18] has calculated several Stark parameters for several species including argon. Since the Stark parameter for Ar I transitions is rather small (typically 10 pm for $n_e \approx 10^{22}$ m^{-3}) and if the heavy particle temperature is low ($T_h \approx 5000$ K corresponds to 4 pm), the measured line profile should be deconvoluted to correct for the instrumental profile of the Fabry-Pérot Interferometer. A spectroscopic set up for the Fabry-Pérot is similar to that used for OES except that the interferometer is positioned at a place where the light path is parallel.

In fig. 10 a typical heavy particle temperature measurement of a plasma jet in argon is shown [19]. These measurements were obtained using the Ar I line profile of the 415.9 nm ($5p - 4s$) transition for $z < 25$ mm and the Ar I line profile of 696.5 nm ($4p' - 4s$) for axial positions larger than 25 mm. Although the line profiles are not Abel inverted, the supersonic expansion and the shock front can be clearly seen (cf. 4). The reason that the 696.5 nm line was not used for the first 25 mm is shown in fig. 11, where the measured line profile for $z = 14$ mm is depicted. As can be seen the line profile is strongly asymmetric. The reason is that the 696.5 nm transition has a large transition probability so that, if the $4s$ (metastable) state is significantly populated, reabsorption occurs over the measured line of sight. The asymmetry is due to the fact that the reabsorption mainly occurs in the cold regions outside of the plasma beam *in* combination with a Stark broadening and shift in the hot plasma jet. Using a simple two region model, i.e., a homogenous plasma region surrounded by a larger, cool (metastable) region, Meulenbroeks et al. [19] could determine the the $4s$ density and temperature of this cold gas. To calculate the Stark broadening and shift for these profiles accurately, the results of the Thomson scattering are used. The result for T_{4s} is shown in fig. 12, where it is compared with the heavy particle temperature of fig. 10. As can be seen the temperature of the cold region gas gradually approaches the heavy particle temperature inside the plasma jet, thus confirming this simple model.

CONCLUSIONS

Three examples of optical diagnostics for high electron density plasmas were discussed. It was shown that by combining the results of these three diagnostics, Thomson-Rayleigh Scattering,

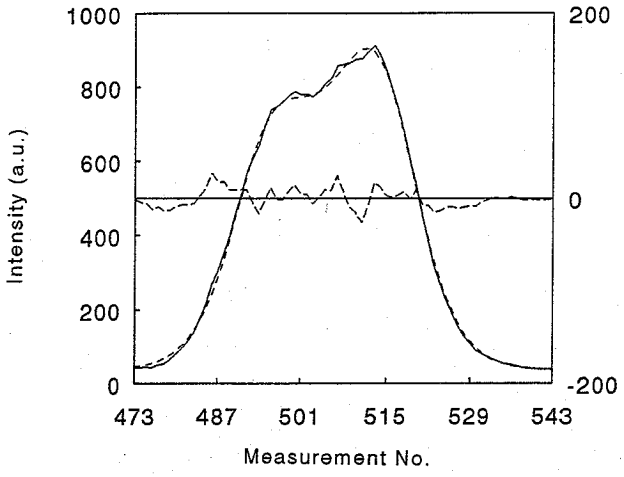

Figure 11. The measured Ar I line profile ($\lambda = 696.5$ nm) at $z = 14$ mm with least mean square fit and 5× magnified residue.$I_{cas} = 45$ A, $Ar - flow = 3500$ ml/min, $p = 40$ Pa.

Optical Emission Spectroscopy and Fabry-Pérot Interferometry, important additional information is gained on, e.g., the metastable density and temperature and the equilibrium state of the plasma.

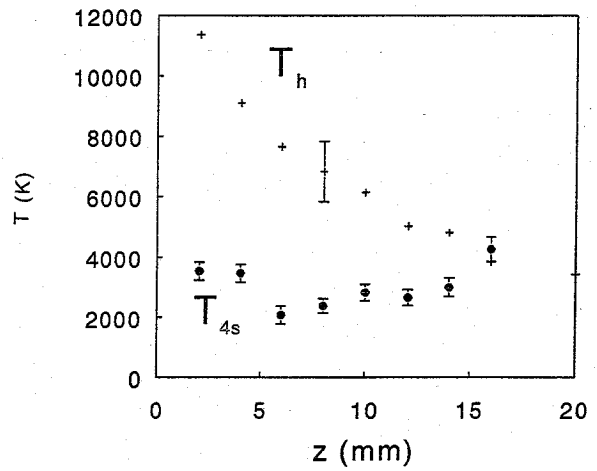

Figure 12. T_{4s} and T_h as a function of the axial position. $I_{cas} = 45$ A, $Ar - flow = 3500$ ml/min, $p = 40$ Pa.

Acknowledgements

We would like to thank M.J.F. van de Sande, H.M.M. de Jong and A.B.M. Hüsken for their skillful technical assistance.

References

1. J.J. Beulens, A.J.M. Buuron, and D.C. Schram, *Carbon deposition using an expanding cascaded arc d.c. plasma*, Surface and Coatings Techn. **47** 401 (1991)
2. G.J. Meeusen, E.A. Ershov-Pavlov, R.F.G. Meulenbroeks, M.C.M. van de Sanden and D.C. Schram, *Emission spectroscopy on a supersonically expanding plasma*, J. Appl. Phys. **71** (1992)
3. M.J. de Graaf, R.P. Dahiya, J.L. Jeauberteau, F.J. de Hoog, M.J.F. van de Sande and D.C. Schram, *Thermal plasma source of hydrogen atoms and ions*, Coll. Phys. **18** C5-387 (1990)
4. J. Sheffield, *Plasma Scattering of Electromagnetic Radiation* (Academic Press, New York, 1975)
5. D.E. Evans and J. Katzenstein, *Laser light scattering in laboratory plasmas*, Rep. Prog. Phys. **32** 207 (1969)
6. A.J.D. Farmer and G.N. Haddad, *Rayleigh scattering measuremnets in a free-burning argon arc*, J.Phys. D **21** 426 (1988)
7. M.C.M. van de Sanden, J.M. de Regt, G.M. Janssen, D.C. Schram, J.A.M. van der Mullen, B. van der Sijde, *A combined Thomson-Rayyeligh scattering diagnostic using an intensified photo diode array*, accepted for publication in Rev. Sci. Instr. (june 1992)
8. P. Jauernik, H. Kempkens and J. Uhlenbusch, *Simultaneous detection of Rayleigh and Thomson scattering signals from a hollow cathode arc plasma*, Plasma Phys. Contr. Fusion **29** 1615 (1987)
9. H.J. Kunze, in *Plasma Diagnostics*, ed. W. Lochte-Holtgreven (North Holland, Amsterdam, 1968)
10. E.E. Salpeter, *Electron density fluctuations in a plasma*, Phys. Rev. **120** 1528 (1960)
11. R.F.G. Meulenbroeks, M.C.M. van de Sanden and D.C. Schram to be published
12. see also article D.C. Schram et al. of this workshop
13. L.M. Biberman, V.S. Vorob'ev and I.T. Yakubov, *Kinetics of Nonequilibrium Low Temperature Plasmas*, (Plenum, New York, 1987)
14. J.A.M. van der Mullen, *Excitation equilibria in plasmas*, Phys. Rep. **191** 109 (1990)
15. see for example: C.A.Kak and M. Slaney, *Principles of Computerized Tomographic Imaging*, (IEEE Press, New York, 1988)
16. M.C.M. van de Sanden, *The expanding plasma jet: Experiments and theory*, thesis University of Technology of Eindhoven, the Netherlands (1991)
17. J.J. Beulens, *Surface modification using a cascade arc plasma source*, thesis University of Technology of Eindhoven, the Netherlands (1991)
18. H.R. Griem, *Spectral Line Broadening by Plasmas*, (Academic Press, New York, 1974)
19. R.F.G. Meulenbroeks, P.A.A. van der Heijden, M.C.M. van de Sanden and D.C. Schram to be published